Journal of Molecular Graphics and Modelling 27 (2009) 571–577

Contents lists available at ScienceDirect

Journal of Molecular Graphics and Modelling

journal homepage: www.elsevier.com/locate/JMGM

Three-dimensional representations of photo-induced electron transfer rates in pyrene-$(CH_2)_n$-N,N′-dimethylaniline systems obtained by three electron transfer theories

Rong Rujkorakarn [a,1], Fumio Tanaka [b,*]

[a] Department of Physics, Faculty of Science, Khon Kaen University, Khon Kaen 40002, Thailand
[b] SC1-413 Department of Chemistry, Faculty of Science, Mahasarakham University, Mahasarakham 44150, Thailand

ARTICLE INFO

Article history:
Received 31 March 2008
Received in revised form 11 September 2008
Accepted 12 September 2008
Available online 25 September 2008

Keywords:
Photo-induced electron transfer
Pyrene-$(CH_2)_n$-N,N′-dimethylaniline
Molecular dynamic simulation
Marcus theory
Bixon and Jortner theory
Kakitani and Mataga theory
Three-dimensional representation of Photo-induced electron transfer rate
Bell shape
Oscillatory shape

ABSTRACT

The observed rates of photo-induced electron transfer (ET) from N,N′-dimethylaniline (DMA) to the excited pyrene (Py) in confined systems of pyrene-$(CH_2)_n$-N,N′- dimethylaniline (P*n*D: $n = 1–3$) were studied by molecular dynamic simulation (MD) and three kinds of electron transfer theories. ET parameters contained in Marcus theory (M theory), Bixon and Jortner theory (BJ theory) and Kakitani and Mataga theory (KM theory) were determined so as to fit the calculated fluorescence intensities with those obtained by the observed ET rates, according to a non-linear least squares method. Three-dimensional profiles of logarithm of calculated ET rates depending on two of three ET parameters, R, ε_0 and $-\Delta G^\circ$ were systematically examined with best-fit ET parameters of P1D. Bell shape dependencies of ET rate were predicted on R and on ε_0, and on $-\Delta G^\circ$ as well, by M theory and KM theory. The profiles of logarithm of ET rate calculated by BJ theory exhibited oscillatory dependencies not only on $-\Delta G^\circ$, but also on R and on ε_0. Relationship between ET state and charge transfer complex was discussed with BJ theory.

1. Introduction

Systematic experimental works on photo-induced electron transfer (ET) in confined systems of pyrene-$(CH_2)_n$-N,N′-dimethylaniline (P*n*D, $n = 1–3$) have been reported by Mataga's group [1–4]. These compounds may be useful as markers for the study of polarity around these compounds in membranes. ET rates were observed by a transient absorption spectroscopy of pyrene (Py) anion produced by ET from N,N′-dimethylaniline (DMA) in the ground state.

ET theories have been reported by many workers [5–13]. However, it is still not clear which theory is best to elucidate experimental ET rates, because every theory contains several ET parameters, and further ET rates depend markedly on them. These ET parameters were quite difficult to evaluate experimentally and theoretically. Most analyses of the observed ET rates have been made with energy gap law [14–18]. In the former work theoretical elucidation on the dynamics of P*n*D in acetonitrile has been worked with KM theory [19], where time-dependent distances between Py and DMA were calculated by MD. In the present work, we have analyzed ET rates of P*n*D by M theory and BJ theory together with KM theory. The dependencies of ET rate on center to center distance, R, between Py and DMA, on ε_0 and on $-\Delta G^\circ$ were examined systematically, using ET parameters contained in three ET theories, determined by a non-linear least squares method. It was predicted that ET rates were often "bell shape" not only along with $-\Delta G^\circ$ (enegy gap law), but also along with R and ε_0 by M theory and KM theory. By BJ theory ET rates were oscillatory in some circumstances.

2. Method of analyses

2.1. MD simulation

Molecular structures of P*n*D are shown in Fig. 1. Charge distributions of the excited P*n*D in acetonitrile were determined

* Corresponding author. Tel.: +66 43 754321; fax: +66 43 754246.
E-mail address: fukoh2003@yahoo.com (F. Tanaka).
[1] Present address: Department of Physics, Faculty of Science, Mahasarakham University.

Abbreviations: ET, photo-induced electron transfer; CT, charge transfer; M theory, Marcus theory; BJ theory, Bixon and Jortner theory; KM theory, Kakitani and Mataga theory; MD, molecular dynamic simulation; MO, molecular orbital; P*n*D, Pyrene-$(CH_2)_n$-N,N′-dimethylaniline; P1D, Pyrene-CH_2-N,N′-dimethylaniline; P2D, Pyrene-$(CH_2)_2$-N,N′-dimethylaniline; P3D, Pyrene-$(CH_2)_3$-N,N′-dimethylaniline; Py, Pyrene; DMA, N,N′-dimethylaniline.

1093-3263/$ – see front matter © 2008 Elsevier Inc. All rights reserved.
doi:10.1016/j.jmgm.2008.09.008

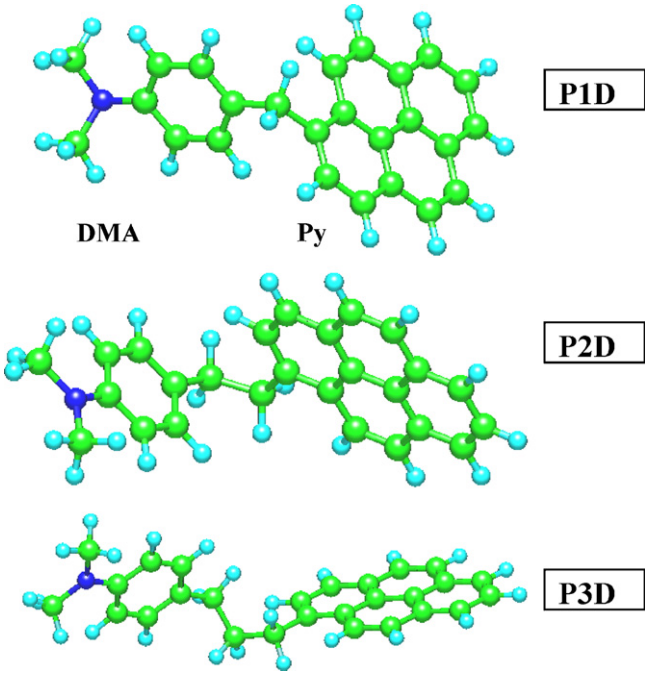

Fig. 1. Molecular models of P*n*D.

with a molecular orbital (MO) software (WinMOPAC PM3: Fujitsu, Japan). Then charge densities of carbon and nitrogen atoms were obtained by unifying with connected hydrogen atoms. Method of MD calculations were described in the previous work [19]. The number of solute was one, and the numbers of acetonitrile molecules were 989 for P3D, 999 for P2D and 1000 for P1D.

2.2. Calculation of ET rate

The ET theories are summarized as follows:
M theory [5–7]:

$$k_{ET} = \nu_0 \sqrt{\frac{\lambda_0}{\lambda_0 + \lambda_s}} \exp\left\{ -\frac{(-\Delta G^\circ - e^2/\varepsilon_0 R + \lambda_0 + \lambda_s)^2}{4(\lambda_0 + \lambda_s) k_B T} \right\} \quad (2.1)$$

where ν_0 is frequency factor, and λ_0 is solute reorganization energies independent of solvent polarity, and R, donor–acceptor distance, $-\Delta G^\circ$ standard free energy gap between reactants and products. k_B and T are Boltzmann constant and temperature. λ_s is known as solvent reorganization energy [5,6] and expressed as

$$\lambda_s = e^2 \left(\frac{1}{2a_1} + \frac{1}{2a_2} - \frac{1}{R} \right) \left(\frac{1}{\varepsilon_\infty} - \frac{1}{\varepsilon_0} \right), \quad (2.2)$$

where e is electron charge, and a_1 and a_2 are radii of donor and acceptor when these reactants are assumed to be spherical, and ε_∞ and ε_0 are optical and static dielectric constants. ε_∞ was 1.89 and ε_0 was 36.6 in acetonitrile. a_1 and a_2 were determined in the following ways: (1) three-dimensional sizes of 1-methylpyrene for Py and *p*-methyl-DMA for DMA were obtained by MO calculations (PM3), (2) the volumes of these molecules were determined as asymmetric rotors, (3) radii of sphere having the same volumes with the asymmetric rotors were obtained. a_1 of Py and a_2 of DMA were 0.240 nm and 0.204 nm, respectively. R between Py and DMA was evaluated as average distance of all pair distances between atoms in Py and atoms in DMA, which were obtained by MD.

BJ theory [8–10]:

$$PQ_i = \sqrt{\frac{\pi}{\hbar^2 \lambda_s k_B T}} V_0^2 \exp\{-\beta(R-\sigma) - S\} \frac{S^i}{i!} \times \exp\left\{ -\frac{(-\Delta G^\circ - e^2/\varepsilon_0 R + \lambda_s + iV_c)^2}{4\lambda_s k_B T} \right\} \quad (2.3)$$

$$k_{ET} = \sum_{i=0}^{n} PQ_i \quad (2.4)$$

where $\hbar = h/2\pi$, h Planck constant. V_0 is electronic interaction energy between the excited Py and DMA at $R = \sigma$. β and σ are constants related to tunneling effect for ET. $S = \lambda_V/V_c$ is the vibronic coupling constant, where λ_V is reorganization energy associated with the average frequency, $V_c = \hbar\langle\omega\rangle$. The value of σ was approximated to be $1/[0.5\{1/a(\text{Py}) + 1/a(\text{DMA})\}]$ and obtained as 0.224 nm. The value of n in the vibronic coupling summation was nine.

KM theory [11-13]:

$$k_{ET} = \frac{\nu_0}{1 + \exp\{\beta(R - R_0)\}} \sqrt{\frac{k_B T}{4\pi\lambda_S}} \exp\left[-\frac{\{-\Delta G^\circ + e^2/\varepsilon_0 R + \lambda_S\}^2}{4\lambda_S k_B T} \right] \quad (2.5)$$

In Eq. (2.5) ν_0 is frequency and β is a coefficient related to ET process. The other constants were common among Eqs. (2.1), (2.3), (2.4) and (2.5). In KM theory the ET process is adiabatic, when $R < R_0$, and non-adiabatic when $R > R_0$.

In M theory, unknown parameters were ν_0, λ_0 and $-\Delta G^\circ$. In BJ theory unknown parameters were V_0, β, λ_V, V_c and $-\Delta G^\circ$. In KM theory unknown parameters were ν_0, β, R_0 and $-\Delta G^\circ$.

2.3. Determination of ET parameters

Observed fluorescence decay function was expressed by Eq. (2.6).

$$F_{obs}(t) = \exp\left(\frac{-t}{\tau_{obs}} \right) \quad (2.6)$$

where τ_{obs} is 11 ps for P3D, 6.1 ps for P2D and 1.7 ps for P1D [4]. Though these τ_{obs}'s were determined by transient absorption spectroscopy, we assumed that fluorescence of P*n*D decayed with these lifetimes. The calculated decay was given as Eq. (2.7) [19,20].

$$F_{calc}(t) = \left\langle \exp\left\{ -\int_0^t [k_0 + k_{ET}(t')] dt' \right\} \right\rangle \quad (2.7)$$

where k_0 is a radiative transition probability of Py, 2.5×10^{-6} ps^{-1}. k_{ET}'s are given by Eqs. (2.1), (2.4) and (2.5). $\langle \ldots \rangle_{AV}$ means averaging procedure of the exponential function in Eq. (2.7). The averaging procedure in P3D was performed by shifting time from 0 to 4.3 ns with time intervals of 1 ps as in the previous work [19]. The averaging procedure in P2D was performed three times by shifting the time from 0 to 1 ns, from 1 to 2 ns and from 2 to 3 ns with time intervals of 0.1 ps. One in P1D was also performed 39 times by shifting time from 0 to 100 ps, from 100 to 200 ps and so on, with intervals of 0.02 ps (see footnote c in Table 1). BASIC program to calculate $F_{calc}(t)$ was a little modified from the former one [19].

The unknown ET parameters were determined so as to obtain the minimum value of χ^2 given by Eq. (2.8), by means of a non-linear least squares method according to Marquardt algorithm.

$$\chi^2 = \frac{1}{N} \sum_{i=1}^{N} \frac{\{F_{obs}(t_i) - F_{calc}(t_i)\}^2}{F_{calc}(t_i)} \quad (2.8)$$

Table 1
Best-fit ET parameters[a].

Theory	PnD	τ_{obs} (ps)	Time range (interval) (ps)	Obtained ET parameter			χ^2
				ν_0 (ps^{-1})	λ_0 (eV)	$-\Delta G^\circ$ (eV)	
M	P3D	11	0–4300 (1)	1012	0.135	1.16	2.96×10^{-4}
	P2D	6.1	0–1000 (0.1)	1011	0.143	1.17	1.89×10^{-5}
			1000–2000 (0.1)	1009	0.151	1.16	1.53×10^{-5}
			2000–3000 (0.1)	1009	0.154	1.17	2.20×10^{-5}
			Average[c] 0–3000 (0.1)	1010 ± 0.6	0.149 ± 0.003	1.17 ± 0.002	$(1.87 \pm 0.193) \times 10^{-5}$
	P1D[b]	1.7	Average[c] 0–3900 (0.02)	994 ± 1.2	0.637 ± 0.013	1.51 ± 0.008	$(1.44 \pm 0.008) \times 10^{-5}$

				V_0 (eV)	β (nm^{-1})	λ_V (eV)	V_c (eV)	$-\Delta G^\circ$ (eV)	χ^2
BJ	P3D	11	0–4300 (1)	0.460	1.23	0.554	0.829	1.00	1.82×10^{-4}
	P2D	6.1	0–1000 (0.1)	0.468	1.23	0.550	0.835	0.991	1.68×10^{-5}
			1000–2000 (0.1)	0.466	1.23	0.551	0.835	0.987	1.36×10^{-5}
			2000–3000 (0.1)	0.464	1.23	0.552	0.834	0.994	2.02×10^{-5}
			Average[c] 0–3000 (0.1)	0.466 ± 0.001	1.23 ± 0.0003	0.551 ± 0.0006	0.835 ± 0.0003	0.991 ± 0.002	$(1.69 \pm 0.189) \times 10^{-5}$
	P1D[b]	1.7	Average[c] 0–3900 (0.02)	0.492 ± 0.005	1.22 ± 0.001	0.543 ± 0.002	0.840 ± 0.001	0.996 ± 0.002	$(1.32 \pm 0.063) \times 10^{-5}$

				ν_0 (ps^{-1})	β (nm^{-1})	R_0 (nm)	$-\Delta G^\circ$ (eV)	χ^2
KM	P3D	11	0–4300 (1)	91.67	6.06	0.577	2.14	1.82×10^{-4}
	P2D	6.1	0–1000 (0.1)	82.07	5.67	0.570	2.12	1.29×10^{-5}
			1000–2000 (0.1)	81.96	5.56	0.564	2.12	1.35×10^{-5}
			2000–3000 (0.1)	82.11	5.56	0.572	2.12	1.34×10^{-5}
			Average[c] 0–3000 (0.1)	82.05 ± 0.05	5.60 ± 0.04	0.569 ± 0.002	2.12 ± 0.00	$(1.345 \pm 0.005) \times 10^{-5}$
	P1D[b]	1.7	Average[c] 0–3900 (0.02)	65.7 ± 3.4	5.66 ± 0.017	0.752 ± 0.015	2.28 ± 0.032	$(1.55 \pm 0.035) \times 10^{-5}$

[a] Solvent was acetonitrile. χ^2 means chi-square between the observed and calculated fluorescence decay functions.
[b] ET parameters were first calculated in every 100 ps time range of MD (altogether 39 ranges) with 0.02 ps time intervals. Then these parameters were taken average among those of 39 time ranges (0–3900 ps range).
[c] Average ± SE.

N is number of data points. Deviations shown in Fig. 4 are expressed by Eq. (2.9).

$$\text{Deviation}\,(t_i) = \frac{\{F_{obs}(t_i) - F_{calc}(t_i)\}}{\sqrt{F_{calc}(t_i)}} \tag{2.9}$$

3. Results and discussion

3.1. Time-dependent changes in the center to center distance and inter-planer angle between Py and DMA in acetonitrile in P2D

Figs. 2 and 3 show time-dependent changes in R and inter-planer angle between Py and DMA, respectively. The mean distance over MD time range was 0.924 nm, which is compared to 1.0 nm in P3D and 0.83 nm in P1D [19]. The mean angle was 22.1°in P2D.

3.2. Fluorescence decays

Fluorescence decay functions of P3D in acetonitrile are illustrated in Fig. 4. The calculated decay was obtained by BJ theory. As shown in Table 1, the value of χ^2 between the observed and calculated intensities by BJ theory was 1.82×10^{-4}. χ^2 values obtained by M theory and KM theory were 2.96×10^{-4} and 1.82×10^{-4}, respectively.

The averaged values of χ^2 over three time ranges in P2D were $(1.87 \pm 0.193) \times 10^{-5}$ by M theory, $(1.69 \pm 0.189) \times 10^{-5}$ by BJ theory and $(1.345 \pm 0.005) \times 10^{-5}$ by KM theory (see Table 1). Averaged χ^2 value of P2D was least in KM theory.

In P1D the averaged values of χ^2 over the entire range of 3.9 ns were $(1.44 \pm 0.008) \times 10^{-5}$ by M theory, $(1.32 \pm 0.063) \times 10^{-5}$ by BJ theory and $(1.55 \pm 0.035) \times 10^{-5}$ by KM theory. Averaged χ^2 value of P1D was least in BJ theory.

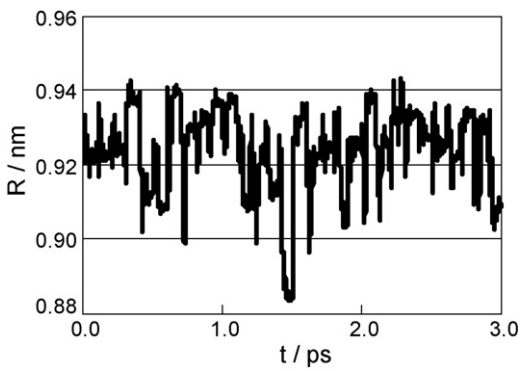

Fig. 2. Time-dependent change in the center to center distance between Py and DMA in P2D in acetonitrile.

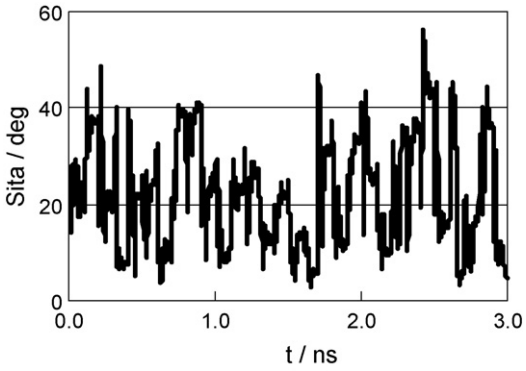

Fig. 3. Time-dependent change in inter-planer angle between Py and DMA rings in P2D in acetonitrile.

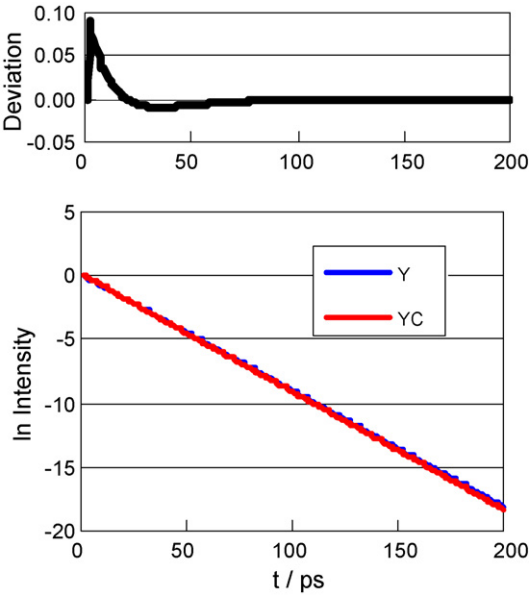

Fig. 4. Fluorescence decays of P3D in acetonitrile by BJ theory. Y and YC represent $F_{obs}(t)$ and $F_{calc}(t)$, respectively. Obtained ET parameters are listed in Table 1. Deviation was obtained by Eq. (2.9).

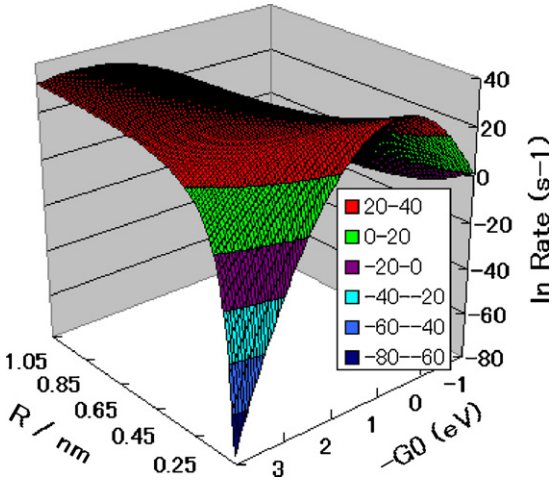

Fig. 5. Dependence of ln k_{ET} on R and $-\Delta G^{\circ}$ obtained by M theory. $-G0$ means $-\Delta G^{\circ}$. Insert shows ln k_{ET} divisions. ET parameters used for the calculation were $\nu_0 = 1.00 \times 10^{15}$ s^{-1} and $\lambda_0 = 0.556$ eV. ε_0 was 36.6.

3.3. Best-fit ET parameters

Best-fit ET parameters are also listed in Table 1. The values of ν_0 obtained by M theory were about 1000 ps^{-1} and almost same among P3D, P2D and P1D. The values of λ_0 were 0.135 eV for P3D, 0.149 eV for P2D, and 0.637 eV for P1D. $-\Delta G^{\circ}$ values were 1.16 eV for P3D, 1.17 eV for P2D, and 1.51 eV for P1D.

The best-fit parameters of V_0 by BJ theory were 0.460 eV for P3D, 0.466 eV for P2D, and 0.492 eV for P1D. The value of β was 1.23 nm^{-1} which was almost same among P3D, P2D, and P1D. The values of λ_V were 0.554 eV for P3D, 0.551 eV for P2D, and 0.835 eV for P1D. The values of V_c were 0.829 eV for P3D, and 0.543 eV for P2D, and 0.840 eV for P1D. $-\Delta G^{\circ}$ values were almost same, 1.00 eV among P3D, P2D, and P1D.

Best-fit parameters of ν_0 by KM theory were 91.67 ps^{-1} for P3D, 82.05 ± 0.05 ps^{-1} for P2D, and 65.7 ± 3.4 ps^{-1} for P1D, which were quite different among three compound. The values of β were 6.06 nm^{-1} for P3D, 5.60 nm^{-1} for P2D, and 5.66 nm^{-1} for P1D. The values of R_0 were 0.577 nm for P3D, and 0.569 nm for P2D, and 0.752 nm for P1D. $-\Delta G^{\circ}$ values were quite similar among the three compounds, 2.14 eV for P3D, 2.12 eV for P2D, and 2.28 eV for P1D.

3.4. Evaluation of ΔG° by MO

We approximate ΔG° as Eq. (3.1),

$$\Delta G^{\circ} = E_{Py}^{anion} + E_{DMA}^{cation} - (E_{Py}^{ex} + E_{DMA}^{gr}) \quad (3.1)$$

where E_{Py}^{anion}, E_{DMA}^{cation}, E_{Py}^{ex} and E_{DMA}^{gr} are total electronic energies of Py anion, DMA cation, Py in the excited singlet state, and DMA in the ground state, respectively. In Eq. (3.1) ΔS° was assumed to be negligible. Total electronic energies were calculated by semi-empirical MO (PM3) calculations. The configuration interaction (CI) was taken into account for the excited Py, Py anion radical, and DMA cation radical. Solvation effect on the total energies in acetonitrile was taken into account by COSMO method. ΔG° were 2.54 eV without inclusion of CI, −0.623 eV with CI = 6 and −1.58 eV with CI = 10. CI = 10 means that number of orbital used for CI calculation is 10. Without CI ΔG° was positive. Experimentally ΔG° was evaluated to be −0.48 eV [3], but accuracy of it was not clear. In the present analysis, the obtained values of ΔG° varied from −1.2 to −1.5 eV by M theory, from −0.99 to −1.0 eV by BJ theory, and −2.1 to −2.3 eV by KM theory.

3.5. Three-dimensional representation of ET rate

Dependencies of ln k_{ET} on two of three parameters, R, ε_0 and $-\Delta G^{\circ}$ were examined. The other parameters were taken from best-fit parameters for P1D (time range, 200–300 ps). Fig. 5 shows dependence of ET rate obtained by M theory at various R and $-\Delta G^{\circ}$. ln k_{ET} rapidly decreased when R became shorter and $-\Delta G^{\circ}$ greater. Bell shape in $-\Delta G^{\circ}$ representation became sharper when R was shorter. The decrease in ln k_{ET} at the shorter R was found when $-\Delta G^{\circ}$ was greater, but not when $-\Delta G^{\circ}$ was negative (Fig. S1). Bell shape in R representation was found when $-\Delta G^{\circ}$ had intermediated value and ε_0 large values (Fig. S2). Fig. 6 shows dependence of ln k_{ET}

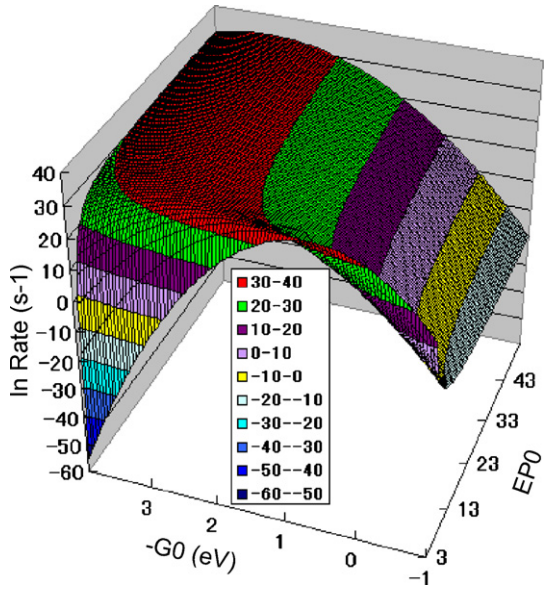

Fig. 6. Dependence of ln k_{ET} obtained on ε_0 and $-\Delta G^{\circ}$ by M theory. EP0 means ε_0. Insert shows ln k_{ET} divisions. R was 0.832 nm. The other parameters were same with those in Fig. 5.

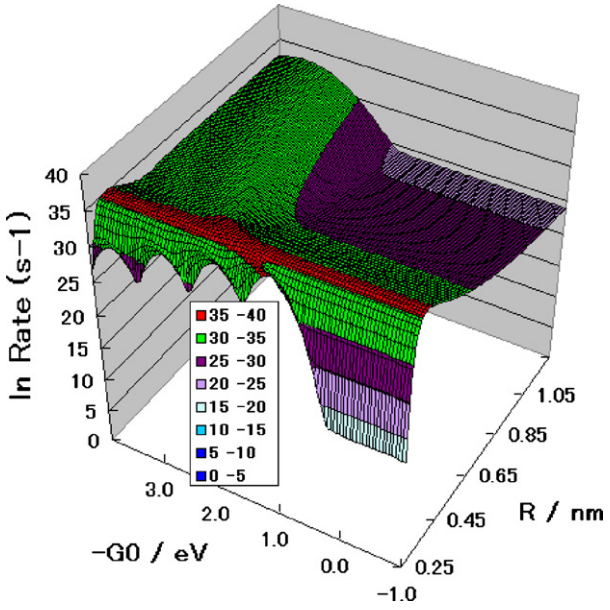

Fig. 7. Dependence of ln k_{ET} on R and $-\Delta G^{\circ}$ obtained by BJ theory. $-G0$ means $-\Delta G^{\circ}$. Insert shows ln k_{ET} divisions. ε_0 was 36.6. The other parameters were V_0 = 0.531 eV, β = 1.21 nm^{-1}, λ_V = 0.528 eV, and V_C = 0.848 eV.

on ε_0 and $-\Delta G^{\circ}$. The maximum value of ln k_{ET} shifted toward greater values of $-\Delta G^{\circ}$ as ε_0 increased. Decrease in ln k_{ET} with ε_0 was found only when $-\Delta G^{\circ}$ was greater, as shown in Fig. S3. ln k_{ET} decreased at $-\Delta G^{\circ}$ = 3.95 eV but increased at $-\Delta G^{\circ}$ = −1.0 eV, as ε_0 decreased. At $-\Delta G^{\circ}$ = 1.40 eV, it showed a bell shape in ε_0 representation. In summary the bell shape of k_{ET} by M theory was predicted along $-\Delta G^{\circ}$, along R at intermediate value of $-\Delta G^{\circ}$ in polar solvents, and along ε_0 at intermediate value of $-\Delta G^{\circ}$.

The dependence of ln k_{ET} on R and $-\Delta G^{\circ}$ was calculated by BJ theory as shown in Fig. 7. The dependence on R and $-\Delta G^{\circ}$ was quite complex. The bell shape in R-representation was also found by BJ theory. It was more profound at less and moderate $-\Delta G^{\circ}$ values (see also Fig. S4). ln k_{ET} was oscillatory along $-\Delta G^{\circ}$

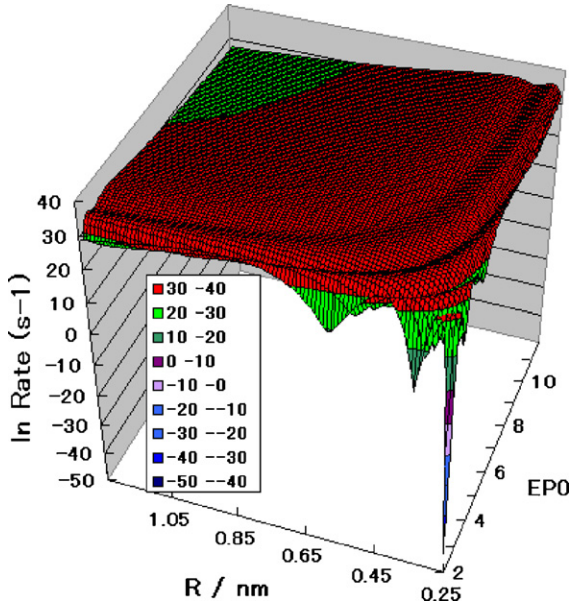

Fig. 8. Dependences of ln k_{ET} on R and ε_0 obtained by BJ theory. EP0 means ε_0. Insert shows ln k_{ET} divisions. $-\Delta G^{\circ}$ was 0.998 eV. The other parameters were same with those in Fig. 7.

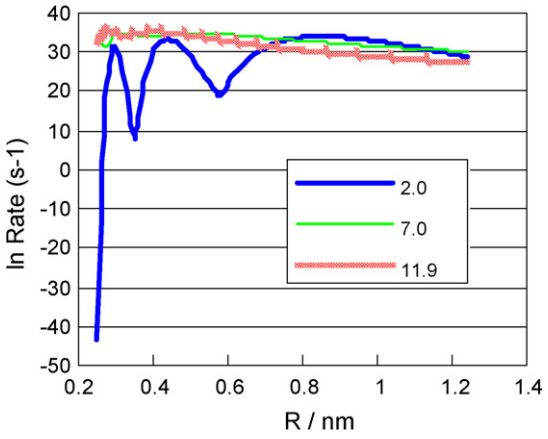

Fig. 9. Dependences of ln k_{ET} on R at various ε_0 obtained by BJ theory. Insert shows ε_0 values. $-\Delta G^{\circ}$ was 0.998 eV. The other parameters were same with those in Fig. 7.

at short donor–acceptor distances. The oscillatory change in ln k_{ET} along $-\Delta G^{\circ}$ was already reported by Bixon and Jortner [8]. It should be noted from Fig. 7 and Fig. S5 that ln k_{ET} did not change with $-\Delta G^{\circ}$ at lower than 0.2 eV at R = 0.25 nm, and lower

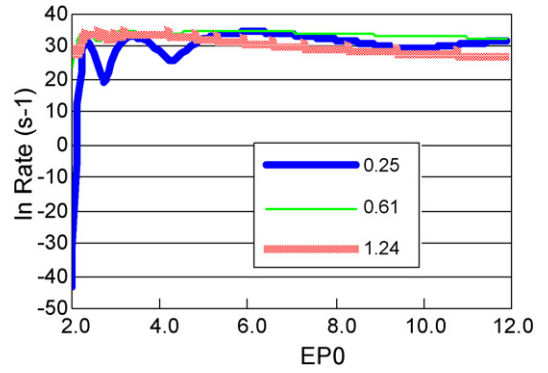

Fig. 10. Dependence of ln k_{ET} on ε_0 at various R obtained by BJ theory. EP0 denotes ε_0. Insert shows R values in nm unit. $-\Delta G^{\circ}$ was 0.998 eV. The other parameters were same with those in Fig. 7.

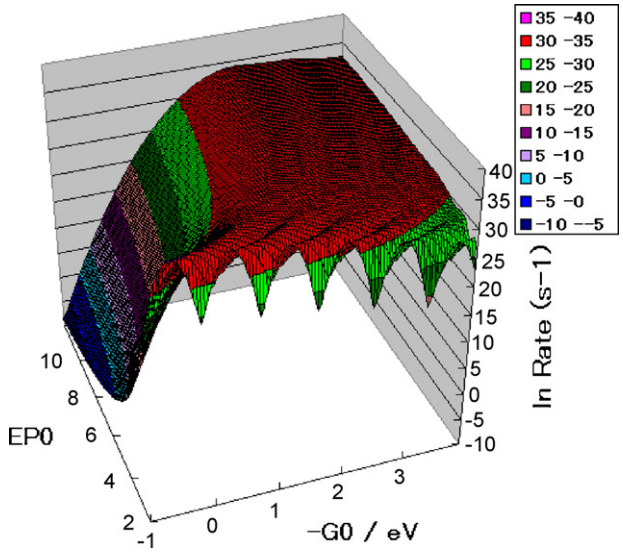

Fig. 11. Dependences of ln k_{ET} on ε_0 and $-\Delta G^{\circ}$ obtained by BJ theory. EP0 and $-G0$ mean ε_0 and $-\Delta G^{\circ}$, respectively. Insert shows ln k_{ET} divisions. R = 0.832 nm. The other parameters were same with those in Fig. 7.

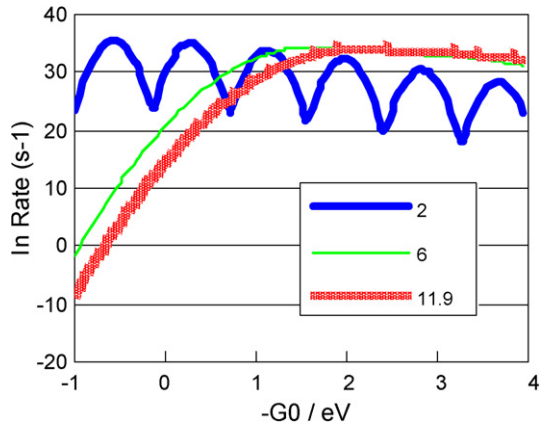

Fig. 12. Dependence of ln k_{ET} on $-\Delta G^{\circ}$ at various ε_0 obtained by BJ theory. $-G0$ means $-\Delta G^{\circ}$. Insert shows ε_0 values. R was 0.832 nm. The other parameters were same with those in Fig. 7.

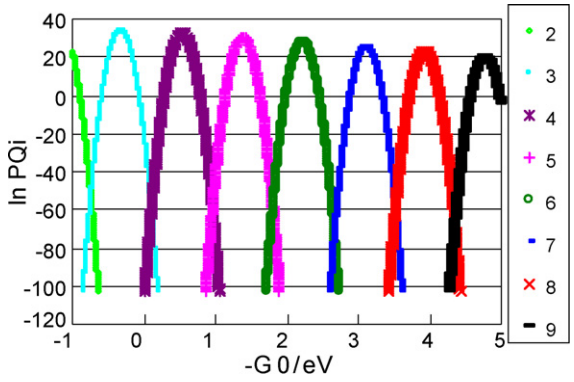

Fig. 13. Dependence of PQ_i on $-\Delta G^{\circ}$ at quantum state i obtained by BJ theory. $-G0$ means $-\Delta G^{\circ}$. Insert shows vibrational quantum state, i. PQ_i are given by Eq. (2.3). PQ_i curves are PQ_2 to PQ_9 from left to right. R = 0.25 nm and ε_0 = 2.0. The other parameters were same with those in Fig. 7.

than 1.8 eV at R = 0.52 nm and 1.24 nm. Fig. 8 shows dependence of ln k_{ET} on R and ε_0. Oscillatory behavior of ln k_{ET} was also predicted along R dependence in non-polar solvent (Fig. 9), and along ε_0 when the distance was short (Fig. 10). Oscillatory

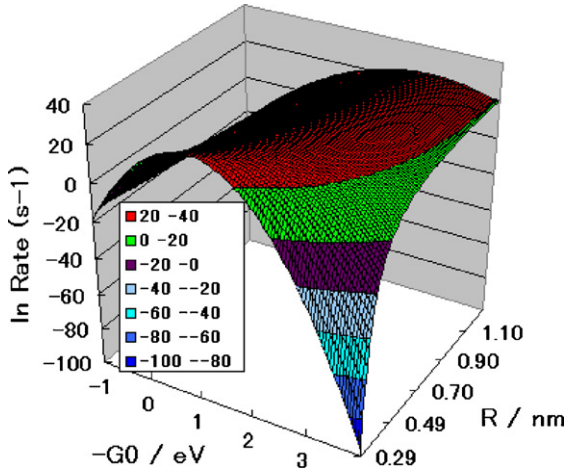

Fig. 14. Dependences of ln k_{ET} on R and $-\Delta G^{\circ}$ by obtained KM theory. $-G0$ means $-\Delta G^{\circ}$. Insert shows ln k_{ET} divisions. The other parameters were $\nu_0 = 9.28 \times 1013$ s^{-1}, $\beta = 5.58$ nm^{-1}, $R_0 = 0.690$ nm, and $\varepsilon_0 = 36.6$.

behavior along ε_0 was more pronounced when the value of $-\Delta G^{\circ}$ was small including negative values (see Fig. S6). Fig. 11 shows dependence of ln k_{ET} on ε_0 and $-\Delta G^{\circ}$. The oscillatory change in ln k_{ET} along $-\Delta G^{\circ}$ was profound at small values of ε_0, but not at ε_0 more than six (see Fig. 12). In summary the bell shape of ln k_{ET} by BJ theory was predicted along R at various $-\Delta G^{\circ}$ values. The oscillatory change of ln k_{ET} was predicted along $-\Delta G^{\circ}$ at shorter distance and along ε_0 at large values of $-\Delta G^{\circ}$ and at short distances, along R at small values of ε_0.

The origin of the oscillatory change in ln k_{ET} by BJ theory was examined as in Fig. 13 and Fig. S7. Fig. 13 shows ET rates from vibrational quantum state, i, according to Eqs. (2.3) and (2.4). PQ_i (i = 2–9) differed very much with the state i. PQ_0 and PQ_1 were negligible. Fig. S7 shows dependencies of PQ_i on ε_0 at various quantum states. The dependences of PQ_i on ε_0 also differed very much with the state i.

ln k_{ET} profiles by KM theory at various values of R and $-\Delta G^{\circ}$ are shown in Fig. 14. $-\Delta G^{\circ}$ value at the maximum ln k_{ET} shifted toward larger as R became longer. The bell shape was predicted along $-\Delta G^{\circ}$, along R at small values of ε_0 and along ε_0 at shorter R (see Fig. S8). $-\Delta G^{\circ}$ value at the maximum ln k_{ET} shifted also toward larger as ε_0 became greater (see Fig. S9). Slight bell shape along ε_0 was predicted at moderate value of $-\Delta G^{\circ}$ (Fig. S10).

4. Conclusion

The present method may be useful to determine ET parameters which have been difficult to obtain experimentally and theoretically. In flavoproteins the donor–acceptor distance-dependent rate of ET was well described by BJ theory and KM theory [21,22], but in P*n*D systems all of three ET theories could reproduce well the observed ET rates. It is of interest that there was no appreciable difference among three ET theories for the elucidation of ET rates in P*n*D in bulk solution.

Bell shape dependence of ET rate was predicted by M theory and KM theory not only on $-\Delta G^{\circ}$ (energy gap law) and on R, but also on solvent polarity. The bell shape of ET rate with donor–acceptor distance implies that ET rate decreases as the distance became shorter than one at the maximum ET rate, despite that the interaction energy between donor and acceptor increases. According to experimental results [1–4], transient absorption spectrum of ET state (ion pair state) is different from one of CT state, and CT state is formed after ET state in moderately polar solvent as acetone, which suggests that physical property between ET and CT states are different. It may be interpreted that as the distance becomes shorter, ET probability decreases, and instead CT state is formed.

The CT state of sandwich type is formed in P3D at shorter R in non-polar solvents [1–4]. In these conditions ET rate by KM theory exhibited bell shape dependence both with R in non-polar solvent and with ε_0 at the shorter distance, but showed oscillatory behavior by BJ theory. Accordingly, in the conditions of CT complex formation the dependencies of ln k_{ET} on R, on ε_0 and on $-\Delta G^{\circ}$ by BJ theory are expected to be completely different among three theories.

Oscillatory dynamics of the excited states of CT complex have been observed in the time domain of sub-picoseconds to picoseconds by photo-bleach recovery in tetracyanoethylene–hexamethylbenzene system [23], by time-resolved fluorescence spectroscopy in various set of donor–acceptor systems [24,25], and in photosynthetic purple bacteria of *Rhodobactor sphaeroides* and *Rhodopseudmonas viridis* [26,27]. Theoretical elucidations of the oscillatory behavior have been also worked [23,28–30]. These theories in the CT complexes may relate to BJ theory in ET, but not to M theory and KM theory.

Appendix A. Supplementary data

Supplementary data associated with this article can be found, in the online version, at doi:10.1016/j.jmgm.2008.09.008.

References

[1] M. Migita, T. Okada, N. Mataga, Y. Sakata, S. Misumi, N. Nakashima, K. Yoshihara, Bull. Chem. Soc. Jpn. 54 (1981) 3304.
[2] T. Okada, M. Migita, N. Mataga, Y. Sakata, S. Misumi, J. Am. Chem. Soc. 103 (1981) 4715.
[3] N. Mataga, in: J.R. Norris, D. Meisel (Eds.), Photochemical Energy Conversion, Elsevier, Amsterdam, 1989, p. 32.
[4] N. Mataga, H. Chosrowjan, S. Taniguchi, J. Photochem. Photobiol. C Rev. 6 (2005) 37.
[5] R.A. Marcus, J. Chem. Phys. 24 (1956) 966.
[6] R.A. Marcus, J. Chem. Phys. 24 (1956) 979.
[7] H. Sumi, R.A. Marcus, J. Chem. Phys. 84 (1986) 4894.
[8] M. Bixon, J. Jortner, J. Phys. Chem. 95 (1991) 1941.
[9] M. Bixon, J. Jortner, J. Cortes, H. Heitele, M.E. Michel-Beyerle, J. Phys. Chem. 98 (1994) 7289.
[10] M. Bixon, J. Jortner, Adv. Chem. Phys. 106 (1999) 35.
[11] T. Kakitani, A. Yoshimori, N. Mataga, Adv. Chem. Ser. 228 (1991) 45.
[12] T. Kakitani, A. Yoshimori, N. Mataga, J. Phys. Chem. 96 (1992) 5385.
[13] T. Kakitani, N. Matsuda, A. Yoshimori, N. Mataga, Prog. React. Kinet. 20 (1995) 347.
[14] J.R. Miller, J.V. Beitz, R.K. Huddeston, J. Am. Chem. Soc. 106 (1984) 5057.
[15] T. Asahi, M. Ohkohchi, R. Matsusaka, N. Mataga, R.P. Zhang, A. Ohsuka, K. Maruyama, J. Am. Chem. Soc. 115 (1993) 5665.
[16] H. Chosrowjan, N. Mataga, Y. Shibata, N. Yoshida, A. Osuka, in: A. Douhal, J. Santamaria (Eds.), Femtochemistry and Femtobiology: Ultrafast Dynamics in Molecular Science, World Scientific Publishing Co. Ltd., New York, 2002, p. 240.
[17] N. Mataga, S. Taniguchi, H. Chosrowjan, Chem. Phys. Lett. 403 (2005) 163.
[18] A. Osuka, G. Noya, S. Taniguchi, T. Okada, Y. Nishimura, I. Yamazaki, N. Mataga, Chem. Eur. J. 6 (2000) 33.
[19] F. Tanaka, S. Keawwangchai, R Rujkorakarn, N. Mataga, Chem. Phys. 348 (2008) 242.
[20] R.M. Hochstrasser, D.K. Negus, Proc. Natl. Acad. Sci. U.S.A. 81 (1984) 4399.
[21] F. Tanaka, H. Chosrowjan, S. Taniguchi, N. Mataga, K. Sato, Y. Nishina, K. Shiga, J. Phys. Chem. B 111 (2007) 5694.
[22] F. Tanaka, R. Rujkorakarn, H. Chosrowjan, S. Taniguchi, N. Mataga, Chem. Phys. 348 (2008) 237.
[23] K. Wynne, C. Galli, R.M. Hochstrasser, J. Chem. Phys. 100 (1994) 4797.
[24] I.V. Rubtsov, K. Yoshihara, J. Phys. Chem. A 101 (1997) 6138.
[25] I.V. Rubtsov, K. Yoshihara, J. Phys. Chem. A 103 (1999) 10202.
[26] M.H. Vos, F. Rappaport, J.-C. Lambry, J. Breton, J.-L. Martin, Nature 363 (1993) 320.
[27] M.H. Vos, M.R. Jones, C.N. Hunter, J. Breton, J.-C. Lambry, J.-L. Martin, Biochemistry 33 (1994) 6750.
[28] K. Ando, H. Sumi, J. Phys. Chem. B 102 (1998) 10991.
[29] S. Ramakrishna, F. Willig, J. Chem. Phys. 115 (2001) 2743.
[30] D.A. Cherepanov, L.A. Krishtalik, A.Y. Mulkidjanian, Biophys. J. 80 (2001) (2001) 103.